

A WAVE EQUATION MODEL FOR FINITE ELEMENT TIDAL COMPUTATIONS

DANIEL R. LYNCH†

Thayer School of Engineering, Dartmouth College, Hanover, NH 03755, U.S.A.

and

WILLIAM G. GRAY†

Water Resources Program, Department of Civil Engineering, Princeton University, Princeton, NJ 08540,
U.S.A.

(Received 20 June 1978)

Abstract—A shallow water wave equation is developed from the primitive two-dimensional shallow water equations. A finite element model based on this equation and the primitive momentum equation is developed. A finite difference formulation is used in the time domain which allows the model to be implicit or explicit while still centered in time. Results obtained with linear triangles and quadratic quadrilaterals are reported, and compare well with analytic solutions. The model incorporates all of the economical advantages of earlier models, and errors due to short wavelength spatial noise are suppressed without recourse to artificial means.

INTRODUCTION

This study is concerned with the description of free surface hydrodynamic circulation in shallow areas, that is, where the vertical fluid depth is much smaller than the horizontal scale of motion. With respect to the regional circulation which occurs within the limits of the continental shelf, this shallow condition generally prevails. The motion considered is dominated by the influence of wind stress and by tidal fluctuations generated by the dynamics of the deeper ocean. The primary mechanical energy flux is horizontal, and the vertical pressure distribution is effectively hydrostatic. The study is limited to non-layered or vertically homogeneous situations wherein it is meaningful to speak of a single vertically averaged fluid velocity. In addition, the fluid density will be assumed to be effectively constant. Under these conditions, it is reasonable to seek a two-dimensional description of the fluid flow. This simplified description can be obtained by integration of the three-dimensional equations of continuity and motion through the fluid depth. This operation has been reviewed by Pritchard[1] and yields the two-dimensional shallow water equations for the conservation of mass and horizontal momentum.

A number of finite element models which solve the shallow water equations have appeared in the literature. A careful reading of this literature indicates that artificial, short wavelength spatial oscillations have been a common source of numerical difficulty. Various techniques have been used to suppress these artificial waves, including the use of viscous terms in the momentum equation (Adey[2], Connor and Wang[3], King *et al.*[4]); numerical smoothing (Brebbia and Partridge[5]); the use of excessive bottom friction (Brebbia and Partridge[6]); and the reporting of computed solutions at element centroids rather than at nodes (Wang and Connor[7]).

Gray and Lynch[8] have illustrated the detrimental effect of these short wavelength disturbances. An efficient leapfrog model was developed and found to compute stable solutions for several test problems. However, when compared with analytic solutions, the leapfrog solutions contain significant short-wavelength errors. The distortion of the computed solution due to these errors is in some cases serious enough to disqualify this model for general operational use unless some form of artificial smoothing is employed.

In an effort to provide natural control of the node-to-node oscillations—i.e., control based on the shallow water equations themselves—Gray and Lynch[8] have developed a semi-implicit model. This model retains most of the computational advantages of the leapfrog model: the solutions for depth and velocity at the unknown time level are uncoupled; the matrices involved

†Assistant Professor.

are stationary and symmetric (and in some cases, diagonal); and no iteration is required. The distinguishing feature of this model is that the primitive equations are operated upon before the finite element discretization is applied, such that second derivatives of depth with respect to space appear in the continuity equation. By comparison with the primitive equation leapfrog model, the semi-implicit model is effective in reducing the short wavelength errors in the computed solution. However, the improvement is not complete, and persistent node-to-node oscillations are still apparent in some of the semi-implicit test results.

Gray and Lynch[9] analyzed a linear wave equation scheme which, like the semi-implicit scheme, contains second derivatives in space which are obtained by operating on the primitive equations. Their analysis predicts that this scheme will both damp and propagate the short wavelength noise, while maintaining high accuracy for the predominant waves. The full nonlinear form of the wave equation is developed below; the finite element method is used to discretize the spatial domain, and solutions for several test problems are obtained by time stepping. Comparisons of computed results with analytic solutions demonstrates the superior behavior of the model.

GOVERNING EQUATIONS

The shallow water equations, in primitive form, are given by Pritchard[1]:

Continuity

$$\frac{\partial H}{\partial t} + \nabla \cdot (H\mathbf{v}) = 0 \quad (1)$$

Momentum

$$\frac{\partial H\mathbf{v}}{\partial t} + \nabla \cdot (H\mathbf{v}\mathbf{v}) + gH\nabla\zeta + \mathbf{f} \times H\mathbf{v} + \tau H\mathbf{v} = H\psi \quad (2)$$

where

$H(x, y, t)$ is the total fluid depth,

$\zeta(x, y, t)$ is the elevation of the free surface above mean sea level,

$h(x, y)$ is the bathymetry function: $h = H - \zeta$,

$\mathbf{v}(x, y, t)$ is the vertically averaged horizontal velocity,

g is gravity,

\mathbf{f} is the vector Coriolis parameter, directed vertically,

$\tau(x, y, t)$ is the friction parameter which accounts for bottom losses (e.g., when using the Chezy model for dissipation, $\tau(x, y, t) = g|\mathbf{v}|/C^2H$, where C is the Chezy coefficient),

ψ accounts for the influence of wind stress and atmospheric pressure variations,

x is positive eastward,

y is positive northward,

t is time, and

∇ is the gradient operator in the horizontal (x, y) plane.

The time derivative and convective terms in (2) may be expanded using the chain rule. Substitution of (1) into the equations and division by H then yields the "non-conservative" form of the momentum equation:

$$\frac{\partial \mathbf{v}}{\partial t} + \mathbf{v} \cdot \nabla \mathbf{v} + g\nabla\zeta + \mathbf{f} \times \mathbf{v} + \tau \mathbf{v} = \psi. \quad (3)$$

The wave equation is obtained by operating on the primitive shallow water eqns (1) and (2). Differentiation of (1) with respect to time yields

$$\frac{\partial^2 H}{\partial t^2} + \nabla \cdot \left(\frac{\partial H\mathbf{v}}{\partial t} \right) = 0. \quad (4)$$

ration is required. The
erated upon before the
depth with respect to
tive equation leapfrog
length errors in the
ersistent node-to-node

like the semi-implicit
rating on the primitive
d propagate the short
nant waves. The full
ent method is used to
are obtained by time
onstrates the superior

d[1]:

(1)

(2)

(3)

(4)

The conservative form of the momentum eqn (2) can be substituted into (4) for $\partial H \mathbf{v} / \partial t$:

$$\begin{aligned} \frac{\partial^2 H}{\partial t^2} - \tau \nabla \cdot (H \mathbf{v}) - H \mathbf{v} \cdot \nabla \tau - \nabla \cdot [\nabla \cdot (H \mathbf{v} \mathbf{v}) + g H \nabla \zeta \\ + \mathbf{f} \times H \mathbf{v} - H \psi] = 0. \end{aligned} \quad (5)$$

Finally, the substitution of the continuity eqn (1) for the term $\nabla \cdot (H \mathbf{v})$ in (5) yields the nonlinear Shallow Water Wave Equation:

$$\frac{\partial^2 H}{\partial t^2} + \tau \frac{\partial H}{\partial t} - \nabla \cdot [\nabla \cdot (H \mathbf{v} \mathbf{v}) + g H \nabla \zeta + \mathbf{f} \times H \mathbf{v} - H \psi] - H \mathbf{v} \cdot \nabla \tau = 0. \quad (6)$$

Equation (6), along with the primitive momentum equation (3), forms the basis of the wave equation model. The finite element method is first used to discretize (6) and (3) in space. A finite difference technique is then used to discretize the time domain.

FINITE ELEMENT DISCRETIZATION IN SPACE

Application of the finite element method to the wave equation is best demonstrated by first obtaining the weak form of eqn (6). The requirement that (6) be orthogonal to the set of functions $\phi_i(x, y)$ yields

$$\begin{aligned} \left\langle \frac{\partial^2 H}{\partial t^2}, \phi_i \right\rangle + \left\langle \tau \frac{\partial H}{\partial t}, \phi_i \right\rangle - \langle \nabla \cdot [\nabla \cdot (H \mathbf{v} \mathbf{v}) + g H \nabla \zeta + \mathbf{f} \times H \mathbf{v} - H \psi], \phi_i \rangle \\ - \langle H \mathbf{v} \cdot \nabla \tau, \phi_i \rangle = 0 \end{aligned} \quad (7)$$

where $\langle \rangle$ denotes an inner product:

$$\langle a, b \rangle \equiv \iint a \cdot b \, dx \, dy \quad (8)$$

and the integration is performed over the entire spatial domain. The third bracketed term in (7) can be integrated by parts:

$$\begin{aligned} - \langle \nabla \cdot [\nabla \cdot (H \mathbf{v} \mathbf{v}) + g H \nabla \zeta + \mathbf{f} \times H \mathbf{v} - H \psi], \phi_i \rangle \\ = \langle [\nabla \cdot (H \mathbf{v} \mathbf{v}) + g H \nabla \zeta + \mathbf{f} \times H \mathbf{v} - H \psi], \nabla \phi_i \rangle \\ - \oint [\nabla \cdot (H \mathbf{v} \mathbf{v}) + g H \nabla \zeta + \mathbf{f} \times H \mathbf{v} - H \psi] \cdot \mathbf{n} \phi_i \, ds \end{aligned} \quad (9)$$

where the surface integral is evaluated on the boundary of the domain, and \mathbf{n} is the unit vector normal to the boundary, directed outward. Equation (9) is simplified by rearranging the conservative momentum equation (2) to the form

$$[\nabla \cdot (H \mathbf{v} \mathbf{v}) + g H \nabla \zeta + \mathbf{f} \times H \mathbf{v} - H \psi] = - \left[\frac{\partial H \mathbf{v}}{\partial t} + \tau H \mathbf{v} \right] \quad (10)$$

and substituting this expression into the surface integral. Thus eqn (7) becomes

$$\begin{aligned} \left\langle \frac{\partial^2 H}{\partial t^2}, \phi_i \right\rangle + \left\langle \tau \frac{\partial H}{\partial t}, \phi_i \right\rangle + \langle [\nabla \cdot (H \mathbf{v} \mathbf{v}) + g H \nabla \zeta + \mathbf{f} \times H \mathbf{v} - H \psi], \nabla \phi_i \rangle \\ - \langle H \mathbf{v} \cdot \nabla \tau, \phi_i \rangle = - \oint \left[\frac{\partial H \mathbf{v}}{\partial t} + \tau H \mathbf{v} \right] \cdot \mathbf{n} \phi_i \, ds. \end{aligned} \quad (11)$$

Following the Galerkin procedure, an approximate solution to (11) is sought in terms of a finite number of basis functions ϕ_j :

$$H(x, y, t) \approx \hat{H} = \sum_{j=1}^N H_j(t) \phi_j(x, y) \quad (12a)$$

$$h(x, y) \approx \hat{h} = \sum_{j=1}^N h_j \phi_j(x, y) \quad (12b)$$

$$\zeta(x, y, t) \approx \hat{\zeta} = \sum_{j=1}^N \zeta_j(t) \phi_j(x, y); \quad \zeta_j = H_j - h_j \quad (12c)$$

$$\mathbf{v}(x, y, t) \approx \hat{\mathbf{v}} = \sum_{j=1}^N \mathbf{v}_j(t) \phi_j(x, y) \quad (12d)$$

$$\tau(x, y, t) \approx \hat{\tau} = \sum_{j=1}^N \tau_j(t) \phi_j(x, y); \quad \tau_j = \frac{g|\mathbf{v}_j|}{C_j^2 H_j} \quad (12e)$$

where N is the number of basis functions.

Substitution of approximations (12) into eqn (11) and rearrangement yields

$$\sum_{j=1}^N \left[\langle \phi_j, \phi_i \rangle \frac{d^2 H_j}{dt^2} + \langle \hat{\tau} \phi_j, \phi_i \rangle \frac{d H_j}{dt} + \langle g \hat{h} \nabla \phi_j, \nabla \phi_i \rangle (H_j - h_j) \right] = r_i \quad (13a)$$

$i = 1, \dots, N$

where

$$r_i \equiv -\langle [\nabla \cdot (\hat{H} \hat{\mathbf{v}} \hat{\nabla}) + g \hat{\zeta} \nabla \hat{\zeta} + \mathbf{f} \times \hat{H} \hat{\mathbf{v}} - \hat{H} \psi], \nabla \phi_i \rangle + \langle \hat{H} \hat{\mathbf{v}} \cdot \nabla \hat{\tau}, \phi_i \rangle - \oint \left[\frac{\partial \hat{H} \hat{\mathbf{v}}}{\partial t} + \hat{\tau} \hat{H} \hat{\mathbf{v}} \right] \cdot \mathbf{n} \phi_i \, ds \quad (13b)$$

In (13), the gravity term $g \hat{H} \nabla \hat{\zeta}$ has been split into the two components $g \hat{h} \nabla \hat{\zeta}$ and $g \hat{\zeta} \nabla \hat{\zeta}$. The term $g \hat{h} \nabla \hat{\zeta}$ is normally much greater than $g \hat{\zeta} \nabla \hat{\zeta}$ and has been retained on the left side of (13) where it will be treated implicitly. The smaller term, $g \hat{\zeta} \nabla \hat{\zeta}$, is nonlinear and has been moved to the right side of (13) where it will be treated explicitly.

Application of the Galerkin-finite element procedure to the momentum eqn (3) yields, in scalar form:

$$\sum_{j=1}^N \left[\langle \phi_j, \phi_i \rangle \frac{d U_j}{dt} + \langle \hat{\tau} \phi_j, \phi_i \rangle U_j \right] = r x_i - \left\langle g \frac{\partial \hat{\zeta}}{\partial x}, \phi_i \right\rangle \quad (14a)$$

$$\sum_{j=1}^N \left[\langle \phi_j, \phi_i \rangle \frac{d V_j}{dt} + \langle \hat{\tau} \phi_j, \phi_i \rangle V_j \right] = r y_i - \left\langle g \frac{\partial \hat{\zeta}}{\partial y}, \phi_i \right\rangle \quad (14b)$$

$i = 1, \dots, N$

where U_j and V_j are the x - and y -components of the velocity \mathbf{v}_j , and

$$r x_i = -\left\langle \left[\hat{U} \frac{\partial \hat{U}}{\partial x} + \hat{V} \frac{\partial \hat{U}}{\partial y} - f \hat{V} - \psi_x \right], \phi_i \right\rangle \quad (14c)$$

$$r y_i = -\left\langle \left[\hat{U} \frac{\partial \hat{V}}{\partial x} + \hat{V} \frac{\partial \hat{V}}{\partial y} + f \hat{U} - \psi_y \right], \phi_i \right\rangle \quad (14d)$$

is sought in terms of a

(12a)

(12b)

(12c)

(12d)

(12e)

yields

$= r_i$

$i = 1, \dots, N$ (13a)

(13b)

its $g\hat{h}\nabla\hat{\zeta}$ and $g\hat{\zeta}\nabla\hat{\zeta}$. The
on the left side of (13)
and has been moved to

itum eqn (3) yields, in

(14a)

$i = 1, \dots, N$ (14b)

(14c)

(14d)

TIME-STEPPING METHOD

A three-level scheme has been chosen for the discretization of (13) and (14) in the time domain. (A minimum of three levels is required by the term d^2H_j/dt^2 in eqn (13).) The time derivatives are replaced with simple second-order finite difference approximations:

$$\left. \frac{dZ}{dt} \right|_k \approx \frac{Z_{k+1} - Z_{k-1}}{2\Delta t} = \frac{\Delta Z_k}{2\Delta t} \quad (15a)$$

$$\left. \frac{d^2Z}{dt^2} \right|_k \approx \frac{Z_{k+1} - 2Z_k + Z_{k-1}}{2\Delta t^2} = \frac{\Delta Z_k - 2(Z_k - Z_{k-1})}{\Delta t^2} \quad (15b)$$

where k is a time level index, and

$$\Delta Z_k \equiv Z_{k+1} - Z_{k-1}. \quad (15c)$$

The remaining terms are all centered in time at level k . The gravity terms in (13) and (14) can be made implicit while still centered in time by use of a time weighting parameter θ :

$$Z_k \approx \frac{\theta}{2}(Z_{k+1} + Z_{k-1}) + (1-\theta)Z_k = \frac{\theta}{2}\Delta Z_k + (1-\theta)Z_k + \theta Z_{k-1} \quad (15d)$$

where θ typically varies from 0 (completely explicit) to 1 (completely implicit).

The friction term in the momentum equation is similarly treated by use of a separate time weighting parameter α .

Substitution of the approximations (15) into eqn (13) yields the matrix equation

$$[A]_k \{\Delta H\}_k = \{RW\}_k \quad (16a)$$

where

$$a_{ij,k} = \langle \phi_j, \phi_i \rangle + \frac{\Delta t}{2} \langle \hat{\tau}_k \phi_j, \phi_i \rangle + \frac{\theta}{2} \Delta t^2 \langle g\hat{h}\nabla\phi_j, \nabla\phi_i \rangle \quad (16b)$$

$$\Delta H_{j,k} = H_{j,k+1} - H_{j,k-1} \quad (16c)$$

$$rw_{i,k} = \Delta t^2 r_{i,k} + 2 \langle (\hat{H}_k - \hat{H}_{k-1}), \phi_i \rangle - \Delta t^2 \langle g\hat{h}\nabla([1-\theta]\hat{\zeta}_k + \theta\hat{\zeta}_{k-1}), \nabla\phi_i \rangle \quad (16d)$$

Use of (15) similarly yields the discrete-time version of the momentum eqns (14):

$$[B]_k \{\Delta U\}_k = \{RMX\}_k \quad (17a)$$

$$[B]_k \{\Delta V\}_k = \{RMY\}_k \quad (17b)$$

where

$$b_{ij,k} = \langle \phi_j, \phi_i \rangle + \alpha \Delta t \langle \hat{\tau}_k \phi_j, \phi_i \rangle \quad (17c)$$

$$\Delta U_{j,k} = U_{j,k+1} - U_{j,k-1} \quad (17d)$$

$$\Delta V_{j,k} = V_{j,k+1} - V_{j,k-1} \quad (17e)$$

$$rmx_{i,k} = 2\Delta t rx_{i,k} - 2\Delta t g \left\langle \frac{\partial}{\partial x} \left(\frac{\theta}{2} \Delta \hat{\zeta} + [1-\theta]\hat{\zeta}_k + \theta\hat{\zeta}_{k-1} \right), \phi_i \right\rangle - 2\Delta t \langle \hat{\tau}_k ([1-\alpha]\hat{U}_k + \alpha\hat{U}_{k-1}), \phi_i \rangle \quad (17f)$$

$$rmy_{i,k} = 2\Delta t ry_{i,k} - 2\Delta tg \left\langle \frac{\partial}{\partial y} \left(\frac{\theta}{2} \Delta \hat{\xi} + [1 - \theta] \hat{\xi}_k + \theta \hat{\xi}_{k-1} \right), \phi_i \right\rangle$$

$$- 2\Delta t \langle \hat{\tau}_k ([1 - \alpha] \hat{V}_k + \alpha \hat{V}_{k-1}), \phi_i \rangle \quad (17g)$$

Boundary conditions are applied exactly as in the semi-implicit model developed by Gray and Lynch[8]. The momentum eqns (17) can be combined into a single composite matrix equation and "rotated" into local normal and tangential coordinates as described by Pinder and Gray[10]. Application of a normal velocity boundary condition at node l is then achieved by discarding the normal momentum equation weighted with respect to ϕ_l ; $(\Delta \mathbf{v} \cdot \mathbf{n})_{l,k}$ may then be specified directly. When depth is specified at a boundary node l , row l of (16) is deleted in favor of the direct specification of $\Delta H_{l,k}$. The surface integral in row l of (16) is required only when node l is a boundary node where the normal or total flux is specified, and in this case the boundary condition information is available for its evaluation. If node l is an interior node, ϕ_l is zero on the boundary and the integral vanishes; if depth is specified at node l , the wave equation is not used at that node.

Equations (16) and (17), as modified by the boundary conditions, constitute the general wave equation time stepping model. Note that (16) does not involve the velocity solution at the unknown time level $k+1$, whereas (17) involves the depth solution at $k+1$. During a single time step, therefore, (16) and (17) may be solved sequentially rather than simultaneously, and without iteration. Equation (16) is solved first for $\{\Delta H\}$. This solution is used to complete the right-hand side of (17), which is then solved for $\{\Delta U\}$, $\{\Delta V\}$.

The presence of the function $\hat{\tau}(x, y, t)$ in $[A]$ and $[B]$ will in general cause these matrices to be nonstationary, which is of course an undesirable feature. However, this complication can always be avoided in the momentum equation by integrating the friction term according to the formula

$$\langle \hat{\tau} \hat{\mathbf{v}}, \phi_i \rangle = \left\langle \sum_{j=1}^N (\tau_j \mathbf{v}_j) \phi_j, \phi_i \right\rangle. \quad (18)$$

Using this integration formula, $[B]$ in eqn (17) becomes

$$b_{ij,k} = \langle \phi_j, \phi_i \rangle + \alpha \Delta t \tau_{j,k} \langle \phi_j, \phi_i \rangle$$

$$= (1 + \alpha \Delta t \tau_{j,k}) \langle \phi_j, \phi_i \rangle \quad (19)$$

and the matrix momentum equations take the form

$$[M] \{\Delta U^*\}_k = \{RMX\}_k \quad (20a)$$

$$[M] \{\Delta V^*\}_k = \{RMY\}_k \quad (20b)$$

where $[M]$ is the stationary mass matrix:

$$m_{ij} = \langle \phi_j, \phi_i \rangle \quad (20c)$$

and

$$\Delta U_{i,k}^* = (\Delta U_{i,k})(1 + \alpha \Delta t \tau_{i,k}) \quad (20d)$$

$$\Delta V_{i,k}^* = (\Delta V_{i,k})(1 + \alpha \Delta t \tau_{i,k}) \quad (20e)$$

$\{RMX\}$ and $\{RMY\}$ are again given by (17f, g), with the friction terms integrated according to (18). Equations (20a, b) may thus be solved for the intermediate values $\Delta U_{i,k}^*$ and $\Delta V_{i,k}^*$. The values of $\Delta U_{i,k}$ and $\Delta V_{i,k}$ are then readily obtained from (20d, e). In this way, the nonstationary feature of the momentum equation is effectively circumvented.

An analogous procedure may be used to obtain a stationary matrix in the wave equation (16) for the special case $\theta = 0$ (i.e. the explicit wave equation model). Use of the integration formula

$$\left\langle \frac{\partial \hat{H}}{\partial t}, \phi_i \right\rangle \approx \left\langle \sum_{j=1}^N \left(\tau_j \frac{dH_j}{dt} \right) \phi_j, \phi_i \right\rangle \quad (21)$$

yields for the matrix $[A]$ in eqn (16)

$$a_{ij,k} = \langle \phi_j, \phi_i \rangle \left(1 + \frac{\Delta t}{2} \tau_{j,k} \right) + \frac{\theta}{2} \Delta t^2 \langle g h \nabla \phi_j, \nabla \phi_i \rangle. \quad (22)$$

When $\theta = 0$, (16-a) becomes

$$[M]\{\Delta H^*\}_k = \{RW\}_k \quad (23a)$$

where $[M]$ is the stationary mass matrix, and

$$\Delta H_{i,k}^* = \Delta H_{i,k} \left(1 + \frac{\Delta t}{2} \tau_{i,k} \right). \quad (23b)$$

The explicit wave equation model combines many attractive features. The solutions for depth and velocity at the unknown time level are uncoupled; the matrices involved are sparse and symmetric; and no iteration is required. Further, use of the integration formulas (18) and (21) causes the matrices to become stationary. The implicit wave equation model ($\theta \neq 0$) also shares these properties, with the single exception that the matrix which must be solved for depth will be non-stationary even if the integration formula (21) is used. For both the explicit and implicit models, further computational savings can be realized by means of lumping the equations, as discussed below.

LUMPED WAVE EQUATION MODEL

In general, when isoparametric elements are used, the inner products in eqns (16) and (17) must be evaluated numerically by an approximate quadrature rule. Traditionally, the method of choice has been Gaussian quadrature, giving the greatest accuracy for a fixed number of integration points (Zienkiewicz[11]). However, Gray and van Genuchten[12] have pointed out that other types of quadrature formulas, when tailored to specific element types, can provide economical alternatives to Gaussian quadrature.

Any element-quadrature combination in which the integration points exactly coincide with the nodes has the effect of lumping the wave equation model. All inner products which contain the term $\langle \phi_j, \phi_i \rangle$ will vanish except when $i = j$. In the case of the momentum equations (17) or (20) the matrices $[B]$ and $[M]$ respectively become diagonal. Thus, the velocities at the unknown time level may be obtained explicitly:

$$\Delta U_{i,k} = r m x_{i,k} / b_{ii,k} \quad (24a)$$

$$\Delta V_{i,k} = r m y_{i,k} / b_{ii,k} \quad (24b)$$

(This result is obtained whether eqn (17) or (20) is used. The approximation (18) is not required in this case.) The coefficients $b_{ii,k}$ are still nonstationary; however since no matrix inversion is required, the recalculation of these coefficients during each time step poses no computational problems. Further, the calculation of the right-hand side arrays $\{RMX\}_k$ and $\{RMY\}_k$ is achieved by effectively one-point quadrature within each element. The requirement that the x - and y -momentum equations be combined into a composite matrix equation and rotated into local normal/tangential coordinates is also eliminated. Boundary conditions on normal velocity can simply be applied after eqns (24) are solved.

The matrix $[A]$ in the wave eqn (16) or (22) will not, in general, be diagonal under this integration procedure, due to the presence of the term

$$\frac{\theta}{2} \Delta t^2 \langle g h \nabla \phi_j, \nabla \phi_i \rangle \quad (25)$$

in a_{ij} . However, for the special case $\theta = 0$ (the explicit wave equation model,) these off-diagonal terms vanish. Thus, in the lumped explicit wave equation model, the depths as well as the velocities are obtained without any matrix inversion.

In order to guarantee convergence, the numerical quadrature must be sufficiently accurate to integrate the area of each element exactly (Strang and Fix [13]). Gray and van Genuchten [12] have shown that the 3×3 Simpson's Rule gives sufficient accuracy for use with isoparametric Lagrangian quadratic quadrilaterals. Gray [14] and Gray and Lynch [8] have used these nine-node quadrilaterals to obtain lumped shallow water models. Other elements whose area can be integrated exactly by nodal quadrature include bilinear quadrilaterals and linear triangles. In both cases, the quadrature assigns equal weight to all of the nodes.

Lumped wave equation results have been obtained using linear triangles and the nine-node quadrilaterals, and are reported below. It should be emphasized that in these models, both the matrices and the right-hand sides of eqns (16) and (17) are lumped automatically by the numerical quadrature. It is believed that this use of nodal quadrature provides a natural and rational basis for lumping. This type of lumping will be referred to as integral lumping to distinguish it from the arbitrary lumping, such as adding up the elements in the row of a matrix, which is typically applied.

FOURIER ANALYSIS

In the linearized, one-dimensional, constant depth case, the wave eqn (6) reduces to

$$\frac{\partial^2 \zeta}{\partial t^2} + \tau \frac{\partial \zeta}{\partial t} - gh \frac{\partial^2 \zeta}{\partial x^2} = 0. \quad (26)$$

This equation can be solved by itself for the surface elevation ζ , regardless of the solution method chosen for velocity. Gray and Lynch [9] have considered the Fourier analysis of the finite element approximation to (26). Lynch [15] extended this analysis to include the linearized momentum equation; the system considered was the finite element equivalent of

$$\begin{bmatrix} \frac{\partial^2}{\partial t^2} + \tau \frac{\partial}{\partial t} - gh \frac{\partial^2}{\partial x^2} & 0 \\ g \frac{\partial}{\partial x} & \frac{\partial}{\partial t} + \tau \end{bmatrix} \begin{Bmatrix} \zeta \\ u \end{Bmatrix} = \begin{Bmatrix} 0 \\ 0 \end{Bmatrix} \quad (27)$$

Both analyses use the time stepping scheme developed herein (eqn (15)), and are limited to one-dimensional linear elements, well removed from the boundaries. Expressions are derived for λ' , the ratio of the numerical solution at time $t + \Delta t$ to that at time t , and compared to the exact analytic value. The results are summarized here:

(a) The wave equation model, like many other three-level models, will admit four values of λ' . Two of these correspond to the physically meaningful progressive and regressive waves, and converge to the exact analytic values of λ as Δt and Δx approach zero independently. These two physical roots depend upon the numerical approximation to the wave eqn (26) alone because of the zero in the upper right corner of the matrix in eqn (27). The other two values of λ' are numerical artifacts and have no analytic counterparts. These numerical roots are determined entirely by the numerical treatment of the terms $\partial u / \partial t + \tau u$ in the momentum equation.

(b) The stability of the physical waves is unconditional when $\theta \geq \frac{1}{2}$. For smaller values of θ , the physical roots are stable when

$$gh \left(\frac{\Delta t}{\Delta x} \right)^2 \leq \frac{1}{3(1-2\theta)}. \quad (28a)$$

For the lumped models, this stability constraint becomes

$$gh \left(\frac{\Delta t}{\Delta x} \right)^2 \leq \frac{1}{(1-2\theta)}. \quad (28b)$$

odel,) these off-diagonal
: depths as well as the

: sufficiently accurate to
van Genuchten[12] have
use with isoparametric
ve used these nine-node
its whose area can be
and linear triangles. In

gles and the nine-node
these models, both the
l automatically by the
provides a natural and
as integral lumping to
in the row of a matrix,

n (6) reduces to

(26)

ardless of the solution
Fourier analysis of the
o include the linearized
valent of

(27)

l5)), and are limited to
expressions are derived
t, and compared to the

ill admit four values of
l regressive waves, and
o independently. These
: wave eqn (26) alone
The other two values of
e numerical roots are
· τu in the momentum

For smaller values of θ ,

(28a)

(28b)

The artificial numerical roots are unconditionally stable for $\alpha > \frac{1}{2}$, and unconditionally unstable for $\alpha < \frac{1}{2}$. This instability is unaffected by lumping. Thus when values of θ less than $\frac{1}{2}$ are used in solving momentum equations (17), (20), or (24), the value selected for α may not be equal to θ but must be greater than $\frac{1}{2}$ to avoid instability.

(c) The propagation accuracy of the wave equation model is by definition based upon the physical values of λ' , and is thus independent of the choice of numerical momentum equation. Plots of the propagation factor for $\theta = 0$ (the explicit case) and $\theta = \frac{1}{2}$ (the limiting unconditionally stable implicit case) are given in Figs. 1 and 2. Comparison with the other schemes considered by Gray and Lynch[9] shows this accuracy to be quite competitive.

(d) The shortest waves which can occur in the numerical solution, those of length $2\Delta x$, are damped when bottom friction is non-zero and also propagated by the wave equation models. It is significant that, within the limits of the Fourier analysis, none of the schemes considered by Gray and Lynch[9] which are based directly on the primitive shallow water equations are capable of either propagating or damping these short waves. The semi-implicit scheme, which requires differentiation of the primitive equations, also fails to propagate these waves, but does introduce damping.

As mentioned in (b) above, there is an unconditional instability associated with the artificial roots, which is avoided where α is greater than $\frac{1}{2}$. Unless otherwise stated, the explicit model results given below were generated with $\alpha = 1.0$. An alternative to this procedure is to evaluate the momentum friction term entirely at time level $k - 1$ (i.e. at time $t - \Delta t$). This approximation is less desirable since the numerical roots are only stable when

$$\tau \Delta t \leq 1.$$

(29)

Further, a loss of accuracy is expected since the friction term is not centered in time. This approach is interesting, however, since it removes the variable τ from the matrix $[B]$ in eqn (17), even when lumping or integration formula (18) is not applied. For the explicit ($\theta = 0$) model, this treatment of the friction term gives a set of momentum equations which are identical to those used in the primitive leapfrog model studied by Gray and Lynch[8].

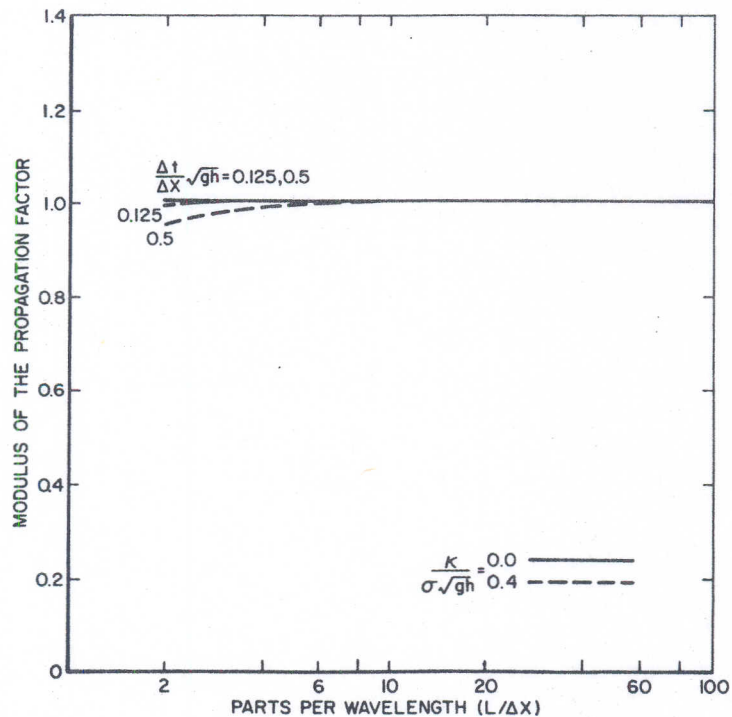


Fig. 1(a)

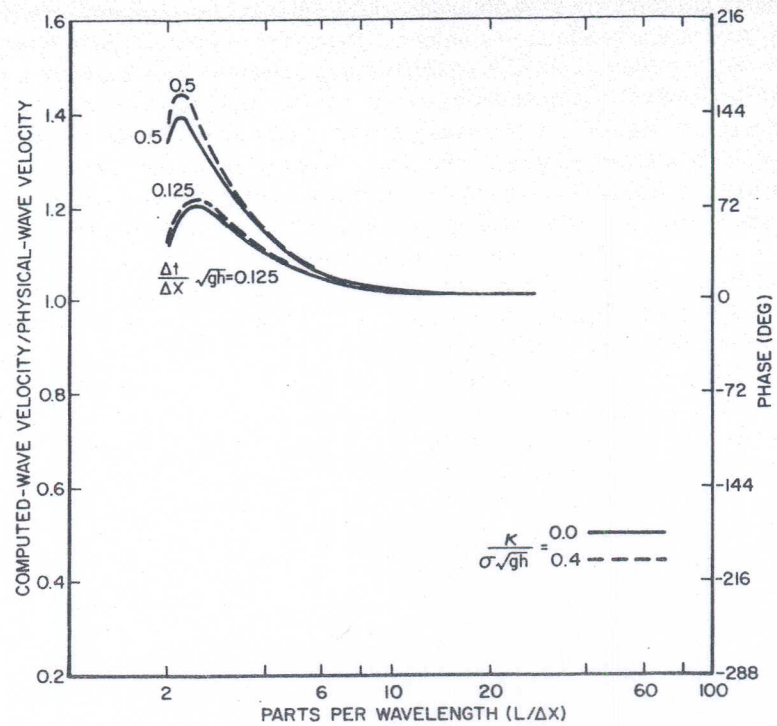


Fig. 1(b)

Fig. 1. Propagation factor for the explicit wave equation scheme.

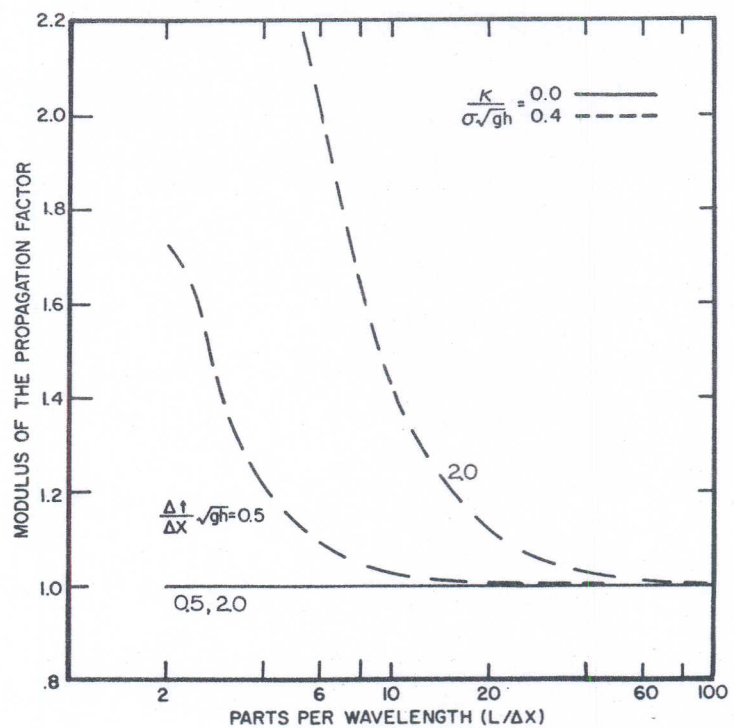


Fig. 2(a)

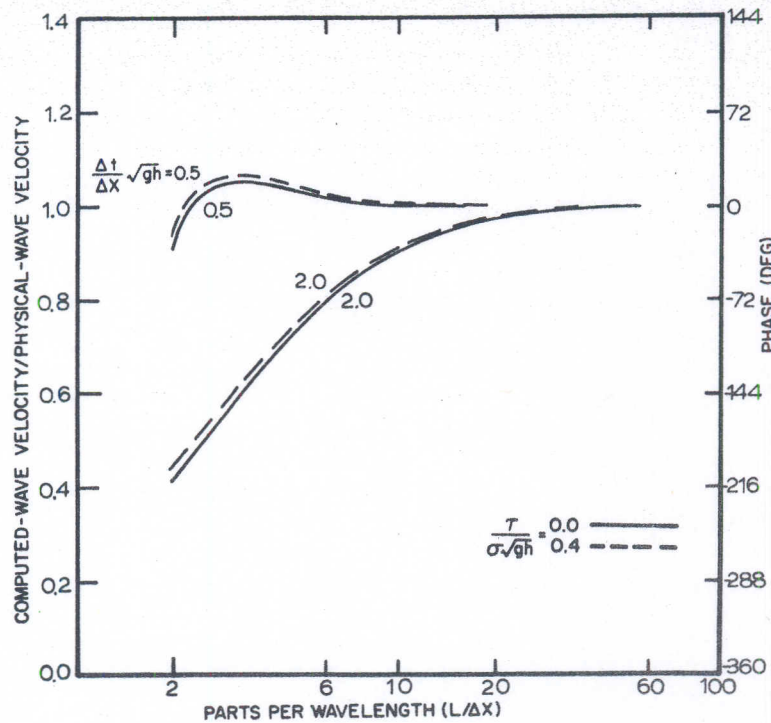


Fig. 2(b)

Fig. 2. Propagation factor for the implicit wave equation scheme, $\theta = 0.5$.

Theoretically, the propagation accuracy of the wave equation models is unaffected by either of these changes, since the physical values of λ' depend upon the numerical wave equation alone. The loss of accuracy when the friction term is uncentered is manifested in the "distribution factor" (Lynch[15], i.e. the relation between the complex amplitudes of depth and velocity for a given travelling wave. Experimentally, this loss of accuracy has not been found to be significant. However, the stability constraint (29) is considered to be important in very shallow regions where τ is expected to be large.

NUMERICAL EXPERIMENTS

Lynch and Gray[16] derived analytic solutions for the two-dimensional linearized shallow water equations for situations involving polar geometry. The solutions include the effects of friction, constant wind stress, and variable bathymetry, and the polar geometry provides curved boundaries. Three of these solutions have been used by Gray and Lynch[16] to test shallow water models and to illustrate the problem of short wavelength oscillations. These three polar test cases are used herein to test the wave equation models.

The physical problem is illustrated in Fig. 3(a). No flow is allowed across the solid boundaries at $r = r_1$, $\theta = 0$, and $\theta = \pi/2$. At $r = r_2$, the surface elevation varies sinusoidally with uniform amplitude and phase. Bathymetry depends upon r alone, and is given by the relation

$$h(r) = h_0 r^n$$

The three test cases differ only in the value of n chosen; constant, linear, and quadratic bathymetry ($n = 0, 1, 2$) will be considered. Coriolis and atmospheric effects are neglected unless otherwise stated. Under these conditions, the analytic solution is independent of θ , and the velocity field is perfectly radial throughout the domain.

Two types of finite elements have been considered. Linear triangles are the simplest two-dimensional elements and yet have several attractive features. Complex geometries are easily accommodated; all inner products can be obtained exactly without numerical integration; and each node has support from a relatively small number of other nodes, which enhances the

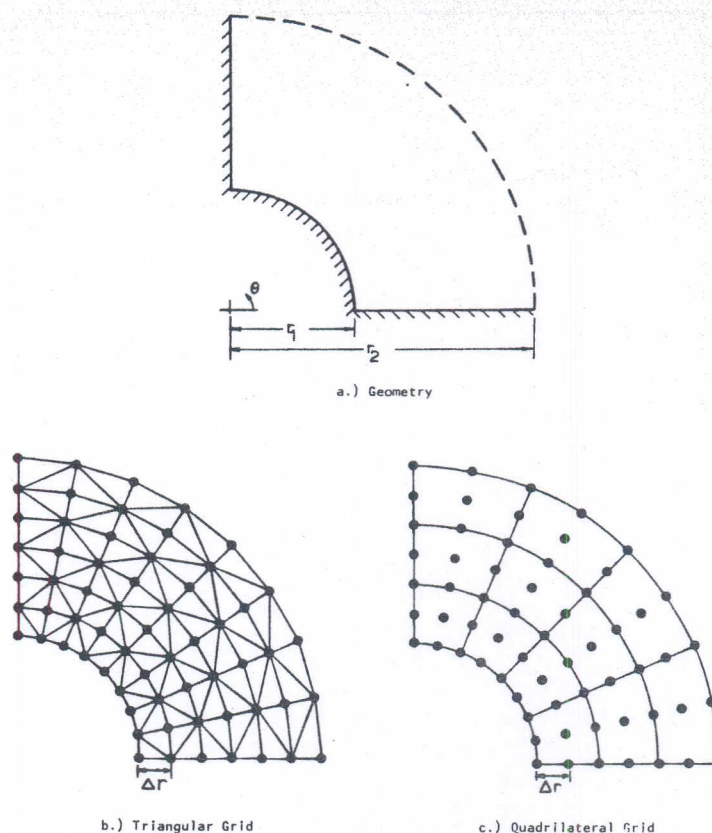


Fig. 3. Polar problem: (a) Geometry; (b) Triangular grid; (c) Quadrilateral grid.

sparseness of the matrices. The triangular grid used for the polar problems is shown in Fig. 3(b).

Quadratic isoparametric Lagrangian quadrilaterals have also been considered, and the grid using these elements is shown in Fig. 3(c). In general, this type of model will be slower in execution than a triangular model, but the use of Simpson's rule quadrature to obtain an integrally lumped scheme makes these elements competitive with the triangles.

Three versions of the wave equation model have been tested: the explicit model, the lumped explicit model, and the lumped implicit model. It should be emphasized that all of the results reported below were obtained from the full nonlinear models (although a constant value of τ was specified). Since the analytic solutions apply only to the linearized equations, small amplitude forcing was used. In all of the tests, computations were begun with the fluid at rest and proceeded until the periodic steady state was reached. Unless otherwise stated, the following parameters apply:

$$\Delta r = 5.0 \times 10^4 \text{ ft.}$$

$$\Delta \theta = \pi/16.$$

$$\text{Period} = 12.4 \text{ hr}$$

$$\Delta t = 0.124 \text{ hr}$$

$$r_1 = 4\Delta r$$

$$r_2 = 10\Delta r$$

$$f = \psi = 0.$$

$$\tau = 10^{-4} \text{ sec}^{-1}$$

$$\text{Amplitude} = 0.1 \text{ ft at } r = r_2$$

For the constant bathymetry case, $h = 30$ ft. For the linear case, h varies from 20 ft at $r = r_1$ to 50 ft at $r = r_2$. The quadratic bathymetry varies from 10 ft at r_1 to 62.5 ft at r_2 . The Courant number, $\Delta t / \Delta t \sqrt{gh}$, is 0.28 for the constant bathymetry case. For the linear and quadratic cases, the Courant number ranges are 0.23–0.36, and 0.16–0.40, respectively.

Explicit wave equation results

Equations (20) and (23) have been solved, with $\theta = 0$ and $\alpha = 1$, for the three polar test problems using the triangular grid. All inner products were evaluated exactly, using the formulas summarized by Zienkiewicz[11] and Pinder and Gray[10]. (Since τ is a constant in these problems, the approximations (18) and (21) are also exact.) The dynamic steady state was reached during the fourth cycle after startup. Qualitatively, the results are quite similar to those obtained by Gray and Lynch[8] with triangular elements. Computed velocities, when converted into polar components, are perfectly radial at every node. The computed solutions along the lines $\theta = 0, 2\Delta\theta, 4\Delta\theta, \dots$ are all equal, but differ slightly from those computed along $\theta = \Delta\theta, 3\Delta\theta, 5\Delta\theta, \dots$. These two different solutions are compared with the analytic solutions in Figs. 4-6 for the constant, linear and quadratic bathymetry cases, respectively. In these figures, the solutions are plotted versus radius at a single point in time, corresponding to the peaking of the forcing at the open sea boundary. The agreement between the numerical and analytic solutions is seen to be quite good. In particular, the node-to-node oscillations in both the circumferential and radial directions are kept under control by the wave equation model. This is particularly apparent when these results are compared with those obtained by Gray and Lynch[8] with the primitive leapfrog and semi-implicit models. (The results reported in this previous paper correspond to the same point in time as those reported herein.)

Two additional problems have been solved with the explicit wave equation model. The constant bathymetry polar test with the triangular grid was repeated, with the addition of Coriolis acceleration equivalent to latitude 41° north:

$$f = 9.57 \times 10^{-5} \text{ sec}^{-1}.$$

All other parameters remained the same. Although no analytic solution is available for this case, the computed solutions are smooth and the velocity fields exhibit the expected curvature. Velocity plots obtained during dynamic steady state are given in Fig. 7 for $t = 475 \Delta t$ and $t = 500 \Delta t$.

The final test of the explicit wave equation scheme again involves the polar geometry of Fig. 3(a) with constant bathymetry. A constant, uniform wind stress was applied in the direction $\theta = \pi/4$. No flux was allowed across the solid boundaries, and the Coriolis effect was neglected.

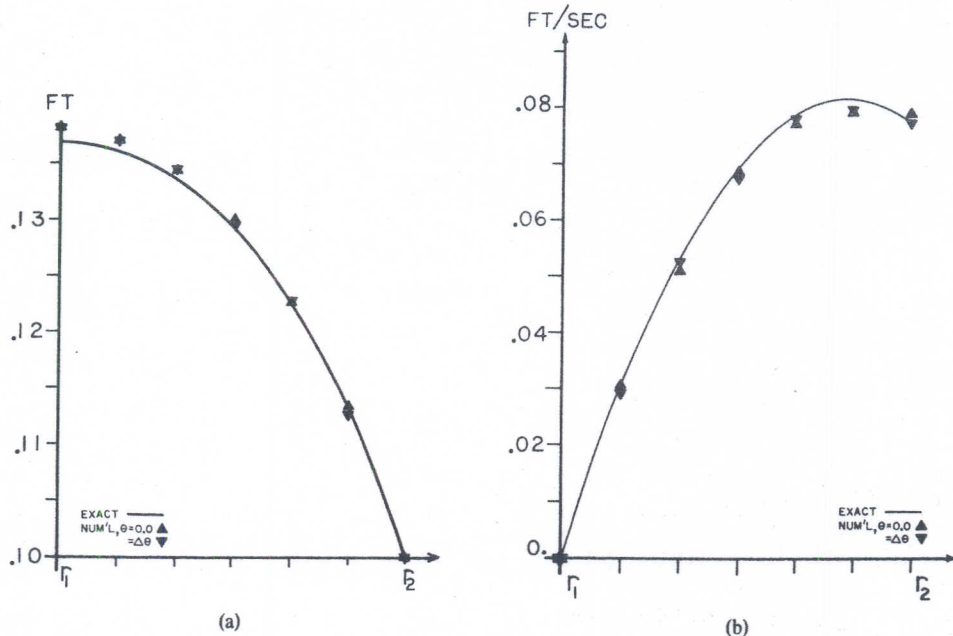
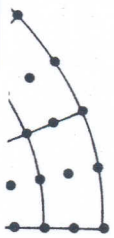


Fig. 4. Explicit wave equation results: triangular grid, constant bathymetry.



Grid

lateral grid.

ms is shown in Fig. 3(b). considered, and the grid model will be slower in quadrature to obtain an e triangles.

explicit model, the lumped ed that all of the results a constant value of τ was quations, small amplitude uid at rest and proceeded the following parameters

ies from 20 ft at $r = r_1$ to .5 ft at r_2 . . The Courant the linear and quadratic tively.

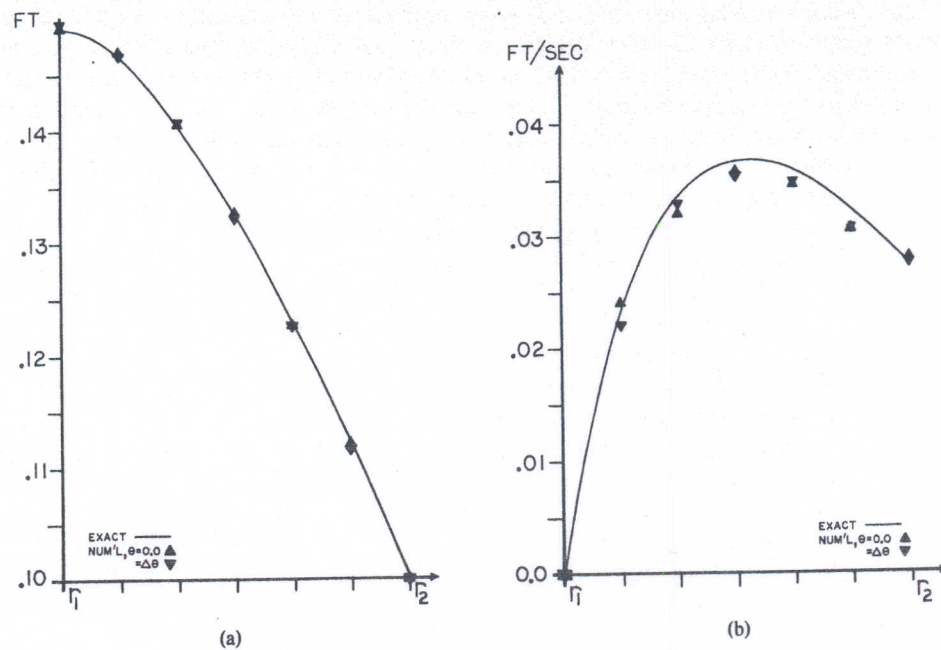


Fig. 5. Explicit wave equation results: triangular grid, linear bathymetry.

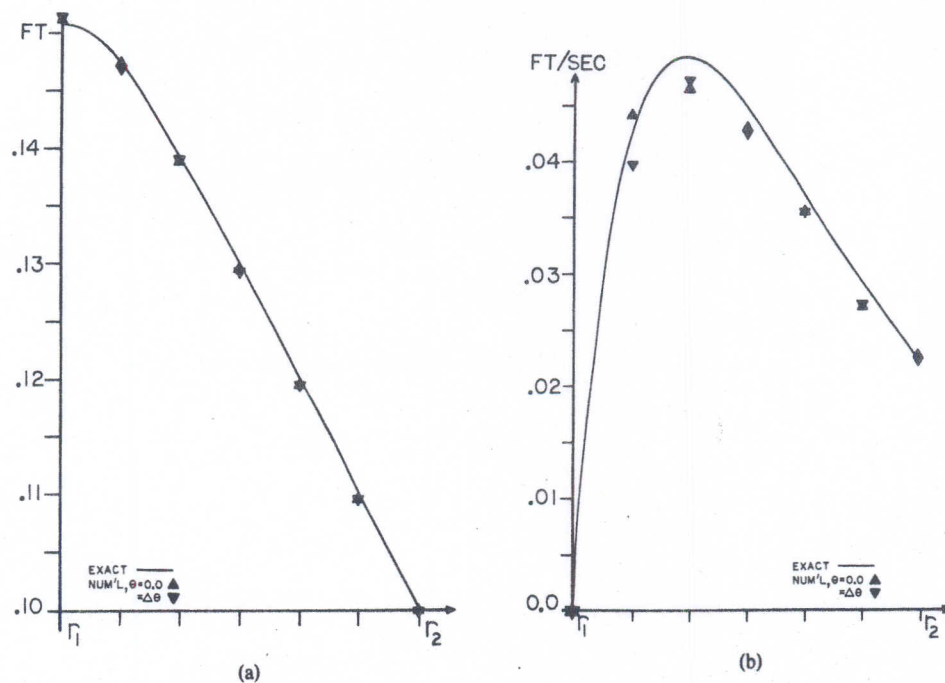
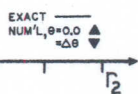
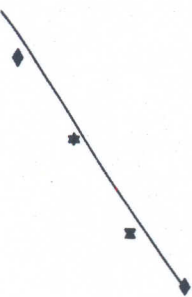


Fig. 6. Explicit wave equation results: triangular grid, quadratic bathymetry.



(b)
hymetry.



(b)
bathymetry.

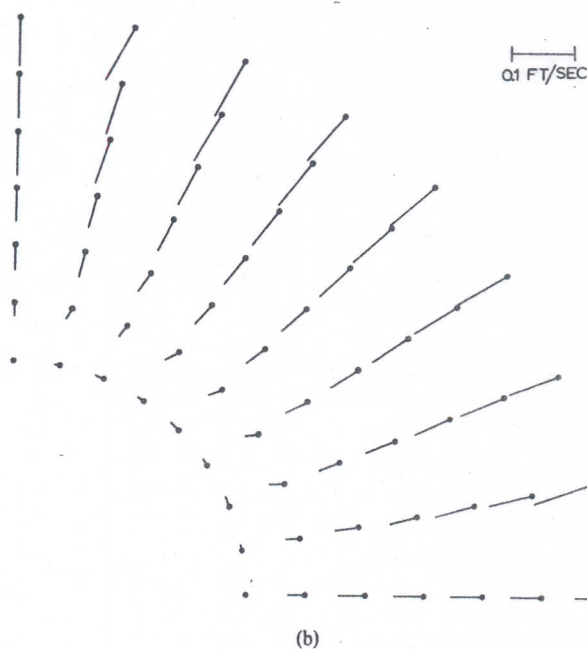
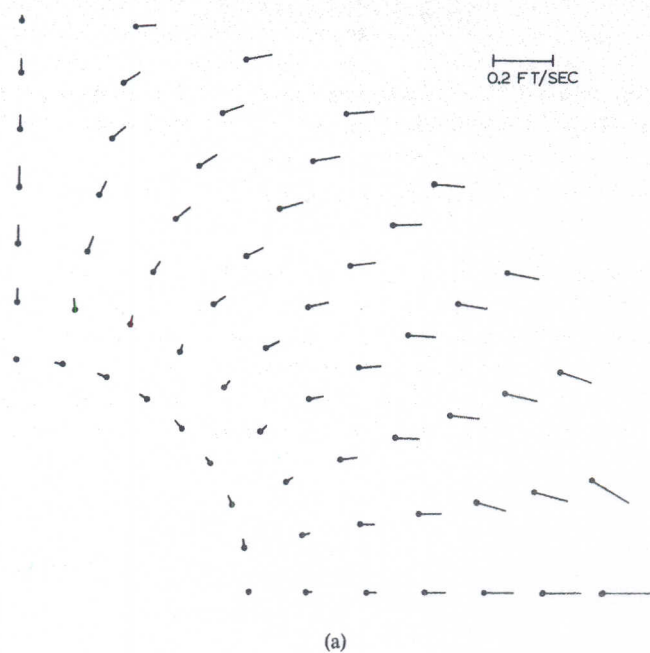


Fig. 7. Explicit wave equation results: triangular grid, constant bathymetry; coriolis effect included.

At $r = r_2$, a steady surface elevation was maintained. For the special boundary condition

$$\zeta(r_2, \theta) = \frac{|W|r_2}{gh} \cos(\theta - \pi/4)$$

where $W = H\psi$ is the wind stress, the linearized analytic solution gives zero velocity everywhere in the steady state. The magnitude of the wind stress used was

$$|W| = 2\sqrt{2} \times 10^{-4} \text{ ft}^2/\text{sec}^2.$$

The model was started impulsively from rest with $\Delta t = 0.124$ hr. After roughly 400 time steps, a condition was reached wherein no further progress toward steady state ($\partial/\partial t = 0$) was possible under single precision conditions with the chosen value of Δt . The computed velocities are everywhere effectively zero. (The actual velocity field is of order 10^{-4} ft/sec, and the random character of this field confirms that it is only a manifestation of round-off error.) The depth results obtained at $t = 500 \Delta t$ are shown in Fig. 8 and the agreement with the analytic solution is quite good.

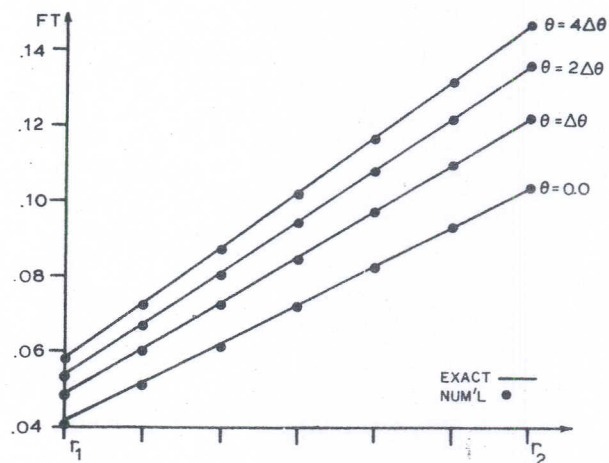


Fig. 8. Explicit wave equation results: triangular grid, constant bathymetry; steady-state wind setup.

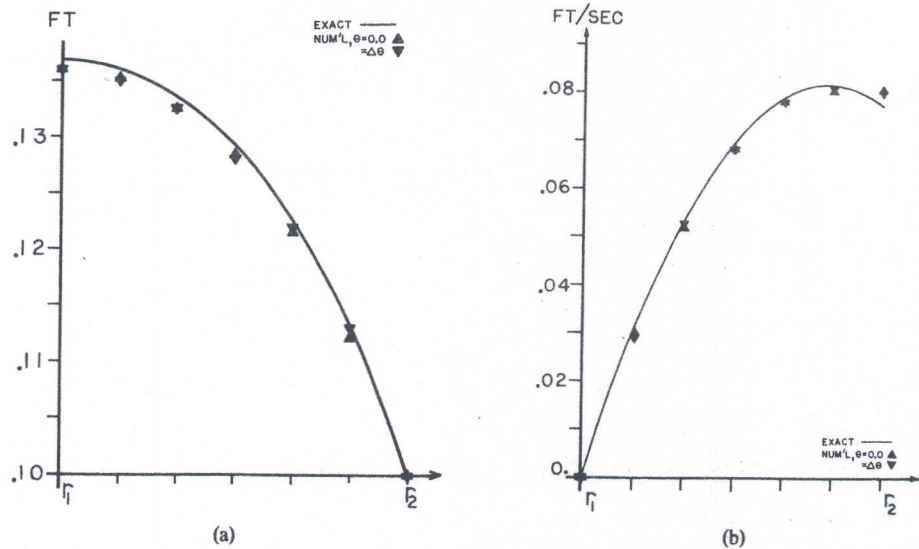


Fig. 9. Lumped explicit wave equation results: triangular grid, constant bathymetry.

Lumped explicit wave equation results

The three polar test problems with sinusoidal forcing, zero Coriolis acceleration and zero wind stress have also been solved using the lumped explicit model, with $\theta = 0$, and $\alpha = 1$. Results obtained with the triangular grid are shown in Figs. 9-11. As in the previous tests where exact integration was used, the computed velocities are perfectly radial at every node. Also, the solutions along the lines $\theta = 0, 2\Delta\theta, 4\Delta\theta$, etc. are identical but slightly different from those at $\theta = \Delta\theta, 3\Delta\theta$, etc. The accuracy of these results is quite good, and comparable to that obtained with exact integration. In fact, in some cases the lumped solutions are marginally superior. However, these differences are not in themselves sufficiently great to support any generalizations on this point.

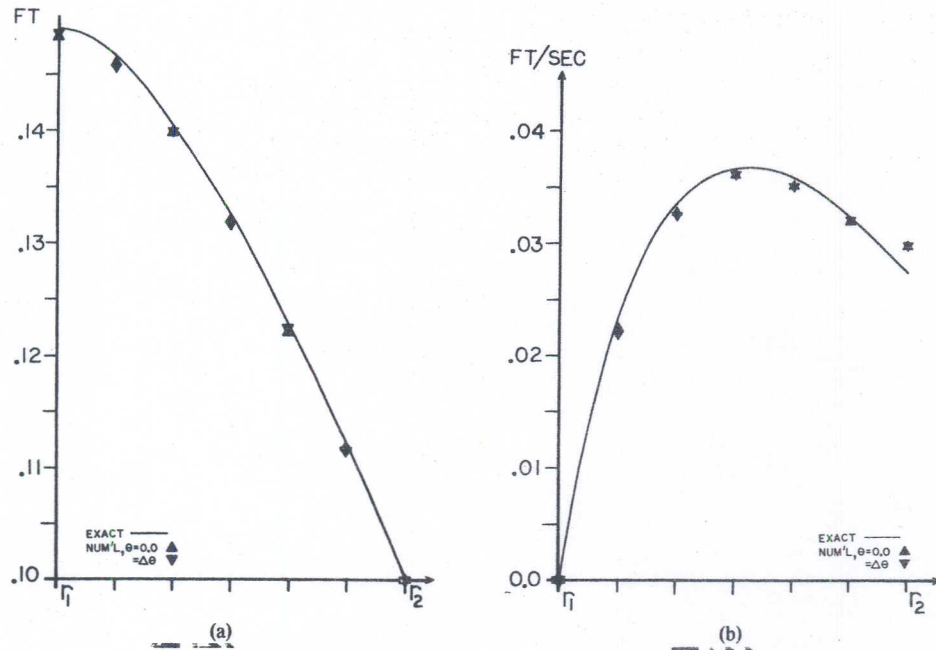


Fig. 10. Lumped explicit wave equation results: triangular grid, linear bathymetry.

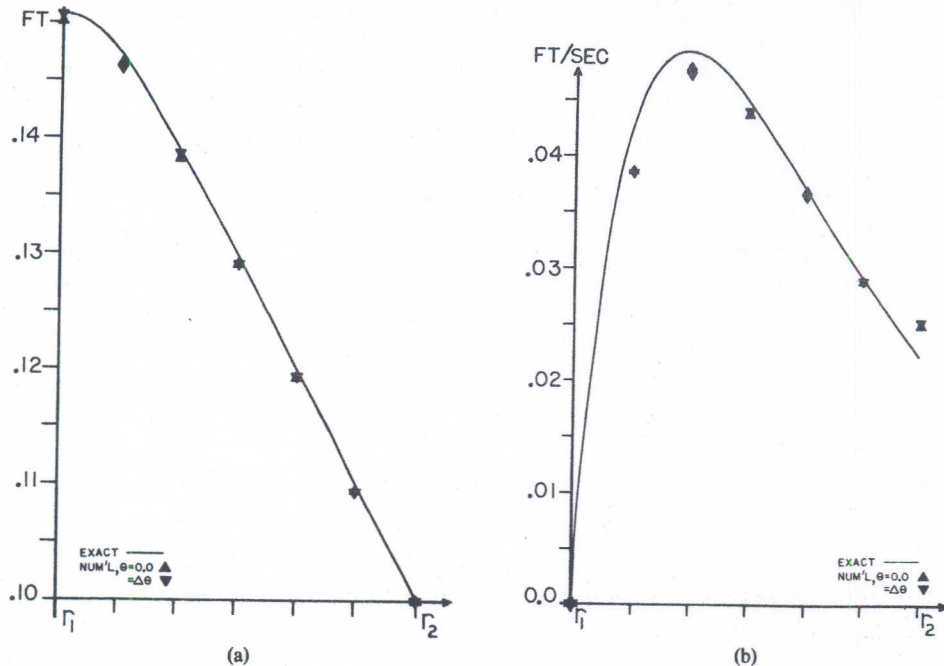


Fig. 11. Lumped explicit wave equation results: triangular grid, quadratic bathymetry.

When the quadratic quadrilateral elements are used (Fig. 3(c)), the computed velocities are again perfectly radial. In contrast to the triangles, however, these elements produce a numerical solution which is independent of θ . (This same qualitative difference between the two element types has been observed by Gray and Lynch[8] in results obtained with earlier models.) The computed results are shown in Figs. 12-14, and compare well with the analytic solutions. Comparison with the earlier results reported by Gray and Lynch also confirms the superiority of the wave equation model over both the primitive leapfrog and the semi-implicit models. In order to emphasize the relative accuracies of these three models, Fig. 15 is a composite of results obtained with the quadrilateral grid. The radial velocity solution obtained with the three models is illustrated for the quadratic bathymetry test case. It is clear from this figure that the wave equation scheme is successful in suppressing the node-node-node oscillations while retaining the underlying solution.

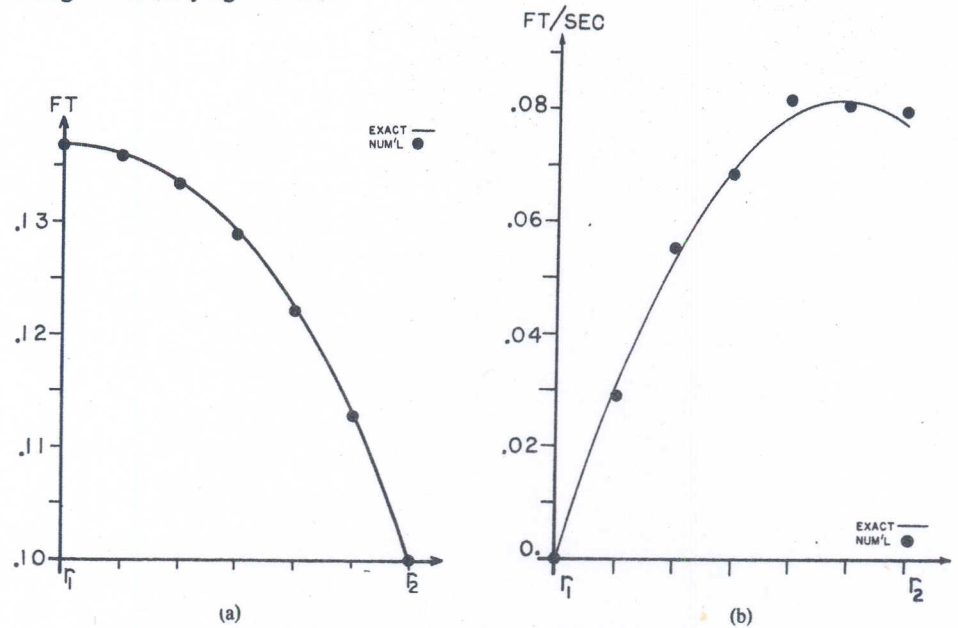


Fig. 12. Lumped explicit wave equation results: quadrilateral grid, constant bathymetry.

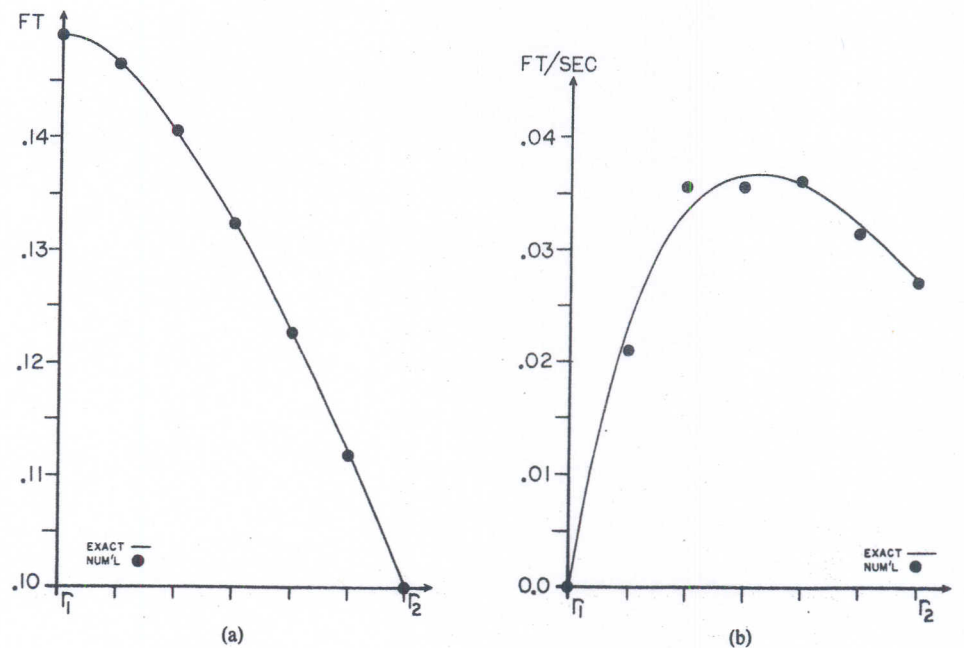


Fig. 13. Lumped explicit wave equation results: quadrilateral grid, linear bathymetry.

computed velocities are
 ts produce a numerical
 tween the two element
 th earlier models.) The
 the analytic solutions.
 confirms the superiority
 semi-implicit models. In
 . 15 is a composite of
 obtained with the three
 rom this figure that the
 ode oscillations while

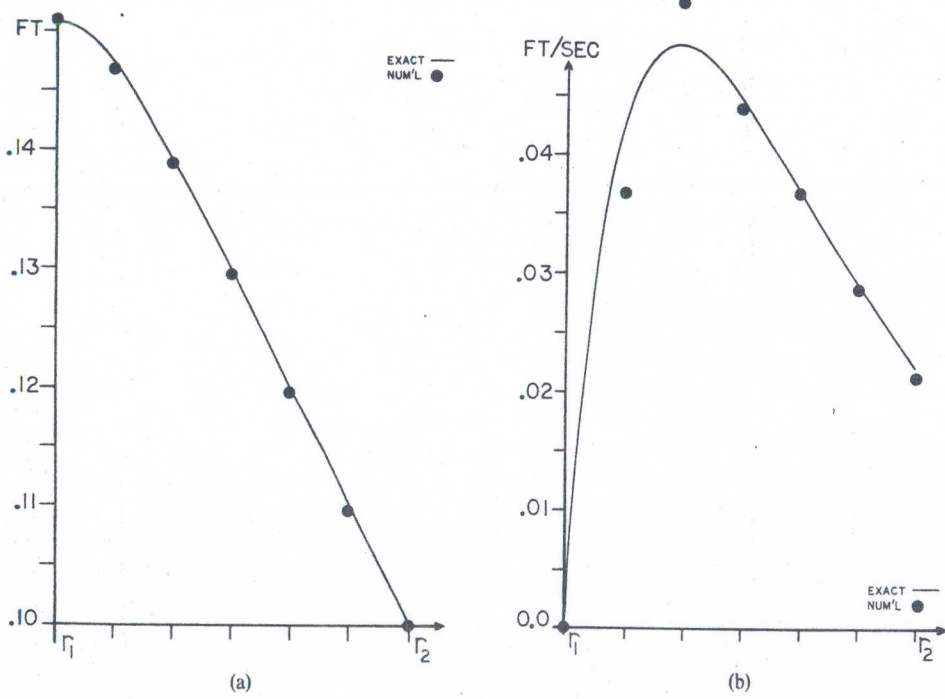
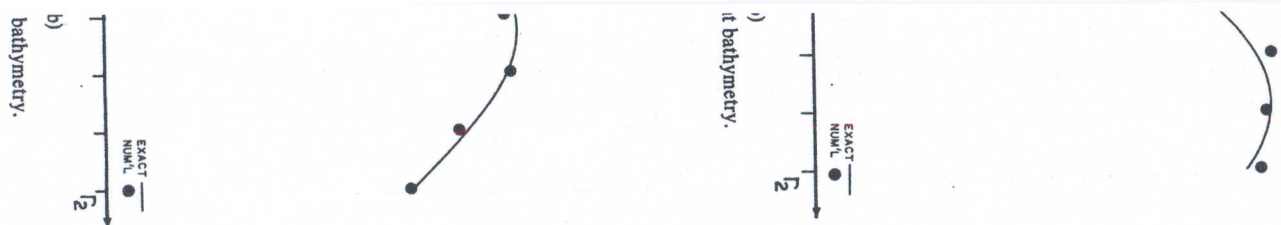


Fig. 14. Lumped explicit wave equation results: quadrilateral grid, quadratic bathymetry.

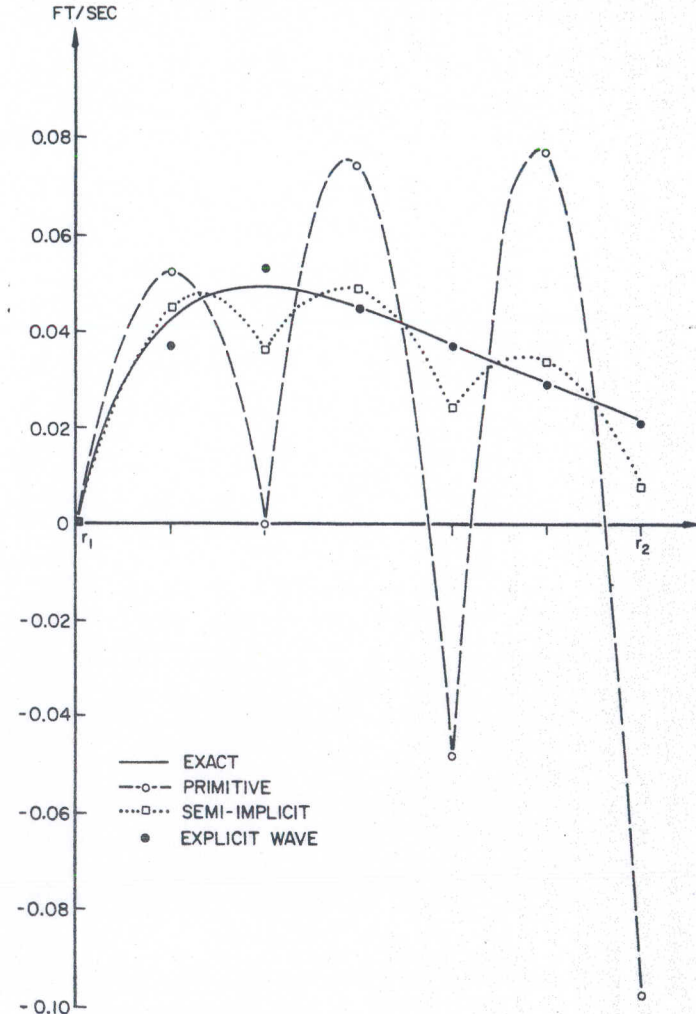


Fig. 15. Comparison of lumped results: quadrilateral grid, quadratic bathymetry; primitive leapfrog, semi-implicit, and explicit wave equation models.

Lumped implicit wave equation results

The Courant number $\Delta t / \Delta r \sqrt{gh}$ in all the preceding examples is within the stability range for the explicit models, and no instability has been observed. For the implicit models, a verification of stability as well as accuracy is desirable. Therefore, the time step has been increased by a factor of five, giving $\Delta t = 0.62$ hr (i.e. 20 time steps per tidal cycle.) Courant number ranges for the three test problems become: constant bathymetry, 1.39; linear, 1.13–1.79; and quadratic, 0.80–2.0. The explicit models are unstable for these problems, as predicted by the Fourier analysis.

The three polar problems with this enlarged time step have been solved with the lumped implicit model, for the triangular grid (Fig. 3(b)). The values of α and θ were both equal to 0.51 (just above the minimum for unconditional stability.) Results are shown in Figs. 16–18, and again

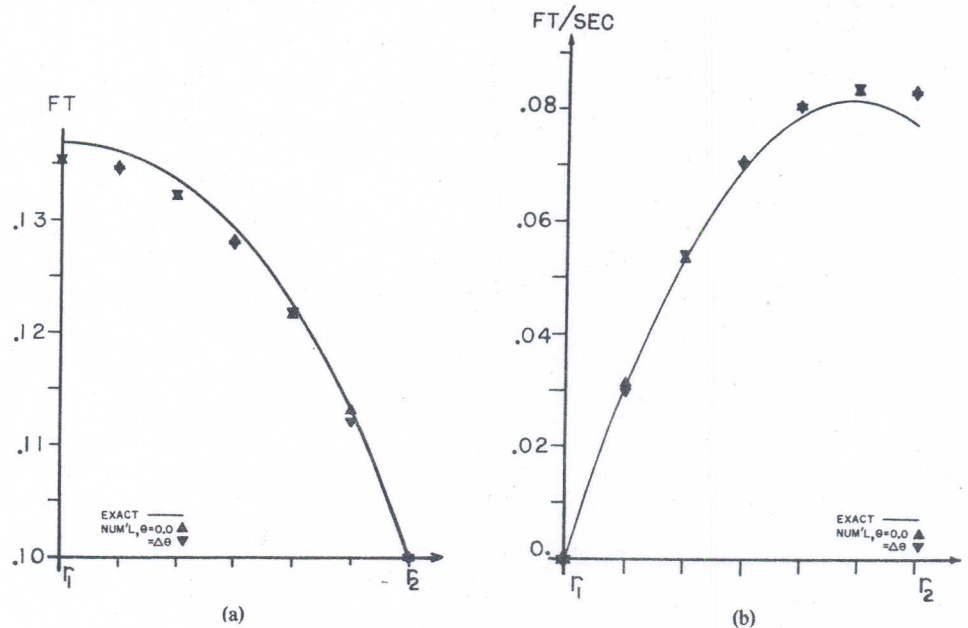


Fig. 16. Lumped implicit wave equation results: triangular grid, constant bathymetry ($\theta = \alpha = 0.51$).

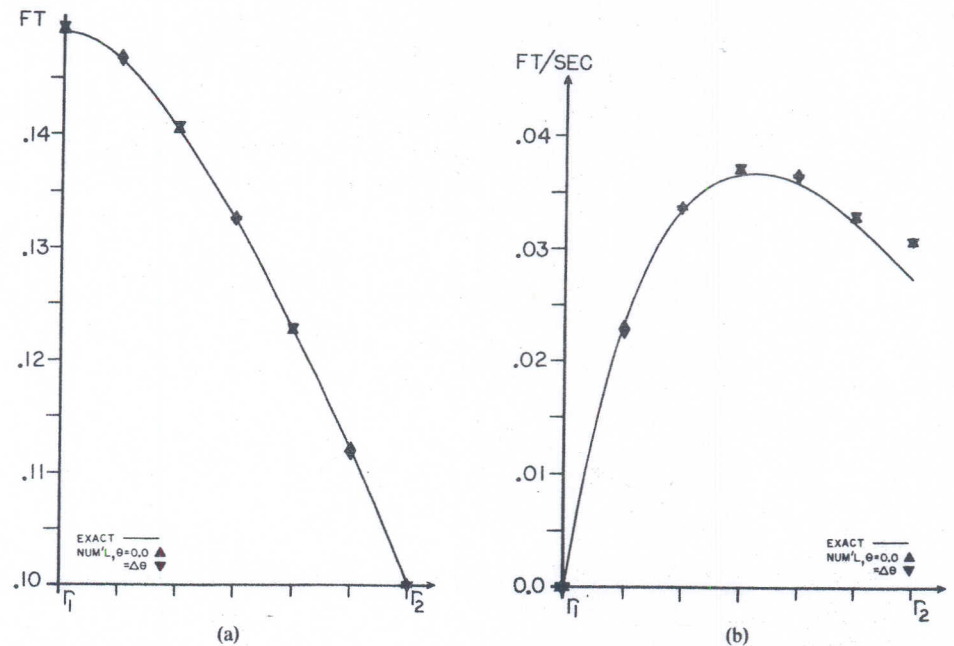
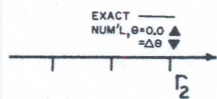


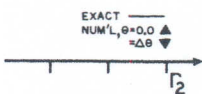
Fig. 17. Lumped implicit wave equation results: triangular grid, linear bathymetry ($\theta = \alpha = 0.51$).

within the stability range of the implicit models, a time step has been chosen for tidal cycle.) Courant number, 1.39; linear, 1.13–1.79; quadratics, as predicted by

solved with the lumped scheme both equal to 0.51 (just Figs. 16–18, and again



try ($\theta = \alpha = 0.51$).



ry ($\theta = \alpha = 0.51$).

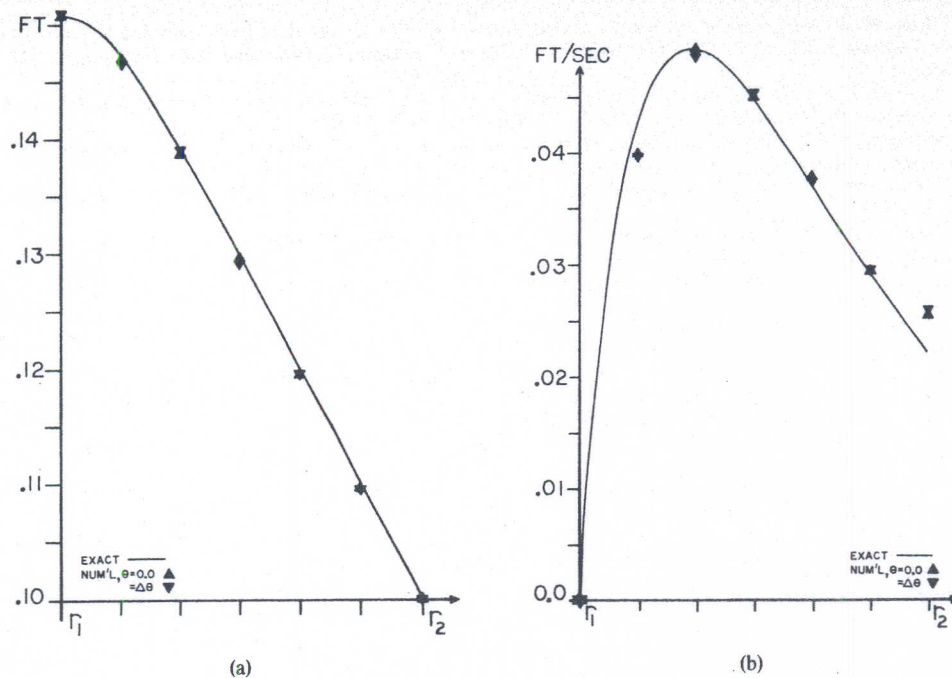


Fig. 18. Lumped implicit wave equation results: triangular grid, quadratic bathymetry ($\theta = \alpha = 0.51$).

the agreement with the analytic solution is excellent. As with all the other results, the dynamic steady state was reached during the fourth cycle after startup, and all computed velocities are perfectly radial. The familiar discretization error associated with the triangles is apparent in the solution, and as the figures show this is kept under control by the wave equation scheme.

CONCLUSION

The wave equation models described above combine most of the economy features which can be realized in a shallow water time-stepping model. The equations for depth and velocity are uncoupled; the matrices are sparse and symmetric, and in most cases stationary; diagonalization is possible by the use of integral lumping; and no iteration is required even for the unconditionally stable implicit version.

A significant feature of these models is that short wavelength errors are suppressed without the use of artificial damping, and without sacrificing the accuracy of the longer physical waves. This is a distinct advantage for general operational use where a hydrodynamic model would be used to drive a transport model. For this case, the presence of short wavelength noise in the flow field is expected to seriously distort the computed contaminant distribution.

The test problems used are believed to represent a realistic spectrum of shallow water conditions. The flexibility of the wave equation models has been illustrated by obtaining accurate solutions (a) with two distinctly different types of elements; (b) with the lumped schemes as well as with exact integration; and (c) with both the implicit and explicit formulations.

Of course, any model must ultimately be tested against field data, and this aspect of the work will be described in a future paper.

Acknowledgement—This work has been supported in part by the United States Geological Survey.

REFERENCES

1. D. W. Pritchard, *Two Dimensional Models*. Chap. 11-2 of *Estuarine Modelling: An Assessment* (Edited by G. H. Ward and W. H. Espey), Water Quality Office, Environmental Protection Agency. NTIS Publication No. PB206-807 (1971).
2. R. A. Adey, *Numerical Prediction of Transient Water Quality and Tidal Motion in Estuaries and Coastal Waters*. Ph.D. Thesis, University of Southampton (March 1974).
3. J. J. Connor and J. D. Wang, Finite element modelling of hydrodynamic circulation. *Numerical Methods in Fluid Dynamics* (Edited by C. A. Brebbia and J. J. Connor), Pentech Press, London (1974).

4. I. P. King, W. R. Norton and K. R. Iceman, A finite element solution for two-dimensional stratified flow problems. *Finite Elements in Fluids*, Vol. 7 (Edited by R. H. Gallagher, J. T. Oden, C. Taylor and O. C. Zienkiewicz), Wiley, London (1975).
5. C. A. Brebbia and P. W. Partridge, Finite element models for circulation studies. *Mathematical Models for Environmental Problems* (Edited by C. A. Brebbia), Wiley, New York (1976).
6. C. A. Brebbia and P. W. Partridge, Finite element simulation of water circulation in the North Sea. *Appl. Math. Modelling*, Vol. 1(2) (1976).
7. J. D. Wang and J. J. Connor, *Mathematical Modelling of Near Coastal Circulation*. MIT Parsons Laboratory Report No. 200 (1975).
8. W. G. Gray and D. R. Lynch, On the Control of Noise in Finite Element Tidal Computations: a semi-implicit approach. *Computers and Fluids* (in press).
9. W. G. Gray and D. R. Lynch, Time-stepping schemes for finite element tidal model computations. *Adv. in Water Resources*, Vol. 1(2) (1977).
10. G. F. Pinder and W. G. Gray, *Finite Element Simulation in Surface and Subsurface Hydrology*. Academic Press, New York (1977).
11. O. C. Zienkiewicz, *The Finite Element Method in Engineering Science*. McGraw-Hill, London (1971).
12. W. G. Gray and M. Th. van Genuchten, Economical alternatives to Gaussian quadrature over isoparametric quadrilaterals, *Intl. J. Numer. Meth. Engrg.* 12(9) (1978).
13. G. Strang and G. J. Fix, *An Analysis of the Finite Element Method*. Prentice-Hall, Englewood Cliffs, New Jersey (1973).
14. W. G. Gray, An efficient finite element scheme for two-dimensional surface water computation. *Finite Elements in Water Resources* (Edited by W. G. Gray, G. F. Pinder and C. A. Brebbia), Pentech Press, London (1977).
15. D. R. Lynch, Finite element solution of the shallow water equations. Ph. D. Thesis, Princeton University (1978).
16. D. R. Lynch and W. G. Gray, Some analytic solutions to the linearized shallow water equations, *J. Hydraulics Division, ASCE* 104(H 10) (1978).